Dynamics of Rotating Discs

Mini Project Report

Submitted by

Subhrajit Bhattacharya (02ME1041)

Under the guidance of

Prof. Anirvan Dasgupta
Dept. of Mechanical Engineering,
IIT Kharagpur.

Department of Mechanical Engineering,
Indian Institute of Technology,
Kharagpur – 721302.

Certificate

This is to certify that thesis entitled “Dynamics of Rotating Discs” submitted by Subhrajit Bhattacharya to Department of Mechanical Engineering, IIT Kharagpur in partial fulfilment of Bachelor degree in Mechanical Engineering, is a bona fide record of work carried out under my supervision and guidance. This fulfils the requirement as per regulation of the institute and meets the standards of submission.

Prof. Anirvan Dasgupta,
Dept. of Mechanical Engineering,
IIT Kharagpur.

Date:

1 Introduction

Rotating discs and similar rotating objects appear in various practical problems in engineering applications. These include rotating shafts, disk clutches, cams, turbine blades, etc. One such specific and rather recent application is rotating data storage devices in computers. Such storage devices, like hard disks and compact disks, generally have to undergo extreme conditions of stresses at extremely high rotation speeds. These speeds typically assume orders of few thousand rotations per minutes. On the other hand with high precision operations in progress and highly sensitive components being present near the rotating disc (e.g. the reading and writing heads), high amplitude of vibrations of the disk cannot be tolerated. The problem takes critical turn when the frequency of rotation of the disc matches with the natural frequencies of vibration of the disc. At these critical frequencies even the slightest of eccentricity in the disk or vibration matching the frequency of rotation of the disk may cause resonance and uncontrollable vibrations in the disk. This situations need to be avoided. One of the approaches to avoid such a situation is to design the disk in such a way so that the natural frequencies of vibration of the disk are increased considerably. Consequently the permeable range of angular rotation of the disk will be much wider. But the material of the disk needs to be chosen suitably so that it can hold the data layer on its surface satisfactorily. This often prevents the choice of a material with high yield strength which could have pushed up the critical frequencies for the disk.
Hence an investigation into the problem seeking alternative ways for strengthening the disk without altering much of its dimensions and material properties and result in an increased critical frequency is highly desirable. The present project work deals with the problem of increasing the natural frequencies and hence the critical frequencies of the disk by inserting thin stiffeners into the disk. Introduction of such stiffeners of higher strength and rigidity though does not affect the properties and performance of the disk reasonably, according to the present analysis it is found that they have successfully increased the natural frequencies of the disk, both in static as well as rotating conditions.
In the present work some analytical treatment of the problem along with some FEM simulation of modal vibration of rotating disks with stiffeners has been made. The addition of radial stiffeners of various shapes showed satisfactory improvement in the results. Along with these some interesting observations have been made regarding the modal shapes on addition of stiffeners.

2 Previous Works

The problem of vibrations of disk is not a new one. It finds it place well in various text books dealing with vibration of structures. Timoshenko [1] has given a detailed analysis of vibration of plates in Cartesian Coordinates. The results have also been obtained in Polar Coordinates by suitable coordinate transformation. However the analysis has been done for the case when the material of the plate is homogeneous and is uniform throughout the solution region. That is, the values of density, Young's modulus and Poisson's ratio remains constant at every point in the solution domain. With these assumptions the governing differential equation for deflection of a plate under static load is in general given by,

$$\Delta\Delta w = \frac{q}{D} \tag{1}$$

where, w = deflection in normal direction,

$D = \frac{Eh^3}{12\left(1-\nu^2\right)}$, with, E = Young's modulus, h = thickness of the plate, ν = Poisson's ratio of the material of the plate,
q = normal load per unit area on the plate.

and $\Delta = \nabla^2$ which assumes the expressions $\Delta = \frac{\partial^2}{\partial x^2} + \frac{\partial^2}{\partial y^2}$ in Cartesian coordinate system and $\Delta = \frac{\partial^2}{\partial r^2} + \frac{1}{r}\frac{\partial}{\partial r} + \frac{1}{r^2}\frac{\partial^2}{\partial \theta^2}$ in Cylindrical Polar coordinates.
A series solution of the differential equation has also been provided in [1].

However the simple form of the equation (1) is radically disturbed once it is assumed that the material properties are functions of space. In fact if stiffeners are inserted into the disk, the material properties can no longer be regarded constant. Under such circumstances the whole analysis needs to be repeated with E, ν and hence, D as functions of the space variables.
Moreover in equation (1) no pre-stressed effects have been considered that may be caused due to the centripetal forces that act on the different parts of a rotating disk. Hence for an analysis of the present problem the pre-stress effects due to rotation need to be considered.
As the present problem deals with circular disk-like plates which are rotating about their axis, it is desirable to obtain the equations in cylindrical polar coordinates. Hence unlike in Timoshenko [1], where the original analysis in Cartesian coordinates have been later transformed to cylindrical polar coordinates, the present approach to the problem has been done in the cylindrical polar coordinates from the very beginning.

3 The Present Analysis

In the present analysis we deal with only the out of plane modes of vibration of the plate/disk. Hence we have only one displacement variable, w, which denotes the vertical displacement of a point on the disk from its un-displaced position. Here w is a function of r, θ and t, where r & θ are the space variables in cylindrical polar coordinates and t is the time.
As we are interested in finding out the natural modes of vibration, we assume that w is a simple harmonic function of time with the same frequency and phase but varying amplitudes for all the points on the disk. That is,

$$w(r,\theta,t) = u(r,\theta)\cdot e^{i\omega_n t} \tag{2}$$

where, ω_n is the frequency of the particular natural mode of vibration.

3.1 Moments on an elemental portion of the disk

We start with the expression for bending and twisting moments on an element of the disk. The expressions for moments per unit length have been given by Timoshenko [1] for any orthogonal coordinate system. We have extended the expression for cylindrical polar coordinates. The bending moments per unit length are given by,

$$M_r = D\left(\frac{1}{\rho_\theta} + \frac{\nu}{\rho_r}\right) \tag{3}$$

$$M_\theta = -D\left(\frac{1}{\rho_r} + \frac{\nu}{\rho_\theta}\right) \tag{4}$$

where, ρ_r and ρ_θ are the radii of curvature along a radial line and tangent respectively and are given by,

$$\rho_r = -\frac{1}{\frac{\partial^2 w}{\partial r^2}} \text{ and } \rho_\theta = -\frac{1}{\frac{1}{r}\frac{\partial w}{\partial r} + \frac{1}{r^2}\frac{\partial^2 w}{\partial \theta^2}}$$

And the twisting moment per unit length is given by,

$$M_{\theta r} = D(1-\nu)\left[\frac{1}{r}\frac{\partial^2 w}{\partial r\,\partial \theta} - \frac{1}{r^2}\frac{\partial w}{\partial \theta}\right] \tag{5}$$

$$\text{and, } M_{r\theta} = -M_{\theta r}$$

Here it may be noted that E, v, and hence D are functions of r and θ.

The following figure shows the moment vectors due to the above acting on an elemental portion of the disk. It may be noted here that the notations used by Timoshenko for M_r and M_θ have been interchanged in the present analysis.

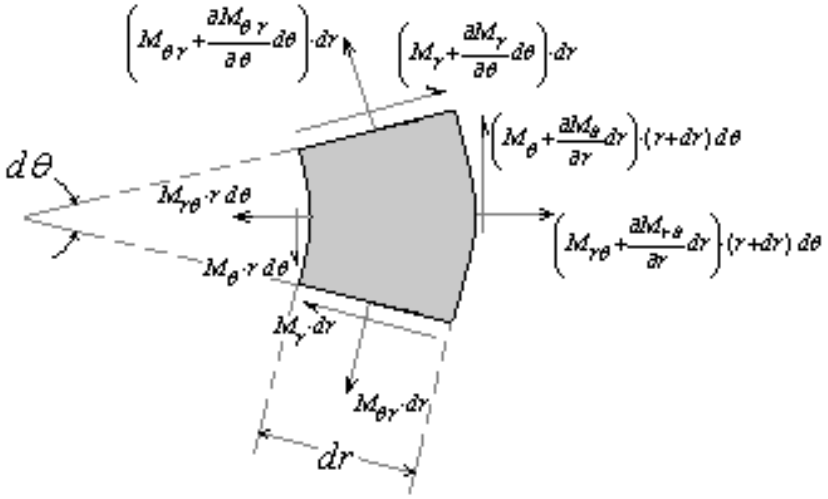

fig – 1

3.2 Shear stresses

Now, figure 2 shows the direction of the shear stresses acting on the element which contribute to the moments along $\boldsymbol{e}_r$ and $\boldsymbol{e}_\theta$ directions.

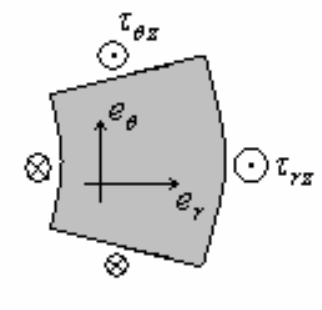

fig – 2

As the moment of inertia of the element about any axis ($\boldsymbol{e}_r$ or $\boldsymbol{e}_\theta$) embedded on it is a differential of order 4, the rotation of the element about the axes can be neglected. Hence we consider equilibrium of the bending & twisting moments and the moments due to the shear forces on the element.

Considering moment about $\boldsymbol{e}_r$,

$$\frac{\partial(rM_{r\theta})}{\partial r}dr\,d\theta \;+\; \frac{\partial M_r}{\partial \theta}dr\,d\theta \;-\; M_{\theta r}dr\,d\theta \;+\; \tau_{\theta z}h\,dr\cdot r\,d\theta \;=\; 0$$

$$\therefore \tau_{\theta z} = -\frac{1}{hr}\left[\frac{\partial M_r}{\partial \theta} + r\frac{\partial M_{r\theta}}{\partial r} + M_{r\theta} - M_{\theta r}\right] \tag{6}$$

And, considering moment about $\boldsymbol{e}_\theta$,

$$\frac{\partial(rM_{\theta})}{\partial r}dr\,d\theta \;+\; \frac{\partial M_{\theta r}}{\partial \theta}dr\,d\theta \;+\; M_r dr\,d\theta \;-\; \tau_{rz}h\,r\,d\theta\,dr \;=\; 0$$

$$\therefore \tau_{rz} = \frac{1}{hr}\left[\frac{\partial M_{\theta r}}{\partial \theta} + r\frac{\partial M_{\theta}}{\partial r} + M_r + M_\theta\right] \tag{7}$$

3.3 Components of Radial and Circumferential stresses due to rotation of the disk

If we consider the disk to be pre-stressed, there will be normal stresses along $\boldsymbol{e}_r$ and $\boldsymbol{e}_\theta$. As the element has a curvature both along $\boldsymbol{e}_r$ and $\boldsymbol{e}_\theta$ directions, there will be components of forces due to σ_r and σ_θ along $\boldsymbol{e}_z$ (figure 3).

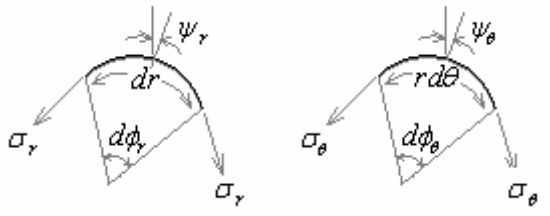

fig - 3

On performing a simple analysis, it can be shown that the components of the forces due to radial and circumferential stresses along $-\boldsymbol{e}_z$ are respectively given by,

$$F_{\sigma_r} = (\sigma_r r\,d\theta\cdot h)\cdot d\phi_r\cdot\cos(\psi_r) = \sigma_r r\,d\theta\cdot h\frac{dr}{\rho_r}\cos(\psi_r) \tag{8}$$

and, $F_{\sigma_\theta} = (\sigma_\theta dr\,h)\cdot d\phi_\theta\cdot\cos(\psi_\theta) = \sigma_\theta dr\,h\frac{r\,d\theta}{\rho_\theta}\cos(\psi_\theta)$ (9)

where, $\psi_r = \tan^{-1}\left(\frac{\partial w}{\partial r}\right)$ and $\psi_\theta = \tan^{-1}\left(\frac{1}{r}\frac{\partial w}{\partial \theta}\right)$.

For a disk with r_i and r_o as internal and external radii respectively and fixed at the inner circumference (as in the present case) and rotating with angular frequency ω, the radial and circumferential stresses are given by,

$$\sigma_r = \frac{3+\nu}{8}\rho\omega^2\left(r_i^2 + r_o^2 - \frac{r_i^2 r_o^2}{r^2} - r^2\right) \tag{11}$$

and, $\sigma_r = \frac{3+\nu}{8}\rho\omega^2\left(r_i^2 + r_o^2 + \frac{r_i^2 r_o^2}{r^2} - \frac{1+3\nu}{3+\nu}r^2\right)$ (12)

3.4 The final equation of motion

Hence, the net force on the element along $\boldsymbol{e_z}$ due to the τ_{rz}, $\tau_{\theta z}$, σ_r and σ_θ causes it to accelerate along $\boldsymbol{e_z}$. Hence, the final equation of motion is given by,

$$\rho h\,dr\cdot r\,d\theta\frac{\partial^2 w}{\partial t^2} = \frac{\partial}{\partial\theta}\left(\tau_{\theta z}h\,dr\right)d\theta + \frac{\partial}{\partial r}\left(\tau_{rz}h\cdot r\,d\theta\right)dr - F_{\sigma_r} - F_{\sigma_\theta}$$

where, ρ is the density of the material and is a function of r and θ.

This gives,

$$\frac{\partial^2 w}{\partial t^2} = \frac{1}{\rho r}\left[\frac{\partial\tau_{\theta z}}{\partial\theta} + r\frac{\partial\tau_{rz}}{\partial r} + \tau_{rz} - \frac{r\sigma_r}{\rho_r}\frac{1}{\sqrt{1+\left(\frac{\partial w}{\partial r}\right)^2}} - \frac{r\sigma_\theta}{\rho_\theta}\frac{1}{\sqrt{1+\left(\frac{1}{r}\frac{\partial w}{\partial\theta}\right)^2}}\right] \quad (10)$$

Now, putting in (10) the expression for w in terms of u and ω_n from (2), and performing all the calculations and simplifications using Mathematica 5.1 the following differential equation was obtained,

$$-\rho r\omega_n^2 u =$$

$$\frac{1}{8}\left(-\frac{r^3\omega^2\rho[r,\theta]\sqrt{1+\frac{u^{(0,1)}[r,\theta]^2}{r^2}}\,u^{(0,2)}[r,\theta]}{r^2+u^{(0,1)}[r,\theta]^2} + \frac{3\,r\,ri^2\omega^2\rho[r,\theta]\sqrt{1+\frac{u^{(0,1)}[r,\theta]^2}{r^2}}\,u^{(0,2)}[r,\theta]}{r^2+u^{(0,1)}[r,\theta]^2} + \right.$$

$$\frac{3\,r\,ro^2\omega^2\rho[r,\theta]\sqrt{1+\frac{u^{(0,1)}[r,\theta]^2}{r^2}}\,u^{(0,2)}[r,\theta]}{r^2+u^{(0,1)}[r,\theta]^2} - \frac{3\,r^3\omega^2\nu[r,\theta]\rho[r,\theta]\sqrt{1+\frac{u^{(0,1)}[r,\theta]^2}{r^2}}\,u^{(0,2)}[r,\theta]}{r^2+u^{(0,1)}[r,\theta]^2} +$$

$$\frac{r\,ri^2\omega^2\nu[r,\theta]\rho[r,\theta]\sqrt{1+\frac{u^{(0,1)}[r,\theta]^2}{r^2}}\,u^{(0,2)}[r,\theta]}{r^2+u^{(0,1)}[r,\theta]^2} + \frac{r\,ro^2\omega^2\nu[r,\theta]\rho[r,\theta]\sqrt{1+\frac{u^{(0,1)}[r,\theta]^2}{r^2}}\,u^{(0,2)}[r,\theta]}{r^2+u^{(0,1)}[r,\theta]^2} +$$

$$\frac{3\,ri^2\omega^2\rho[r,\theta]\sqrt{\frac{r^2+u^{(0,1)}[r,\theta]^2}{r^2}}\,u^{(0,2)}[r,\theta]}{r^3+r\,u^{(0,1)}[r,\theta]^2} + \frac{3\,ro^2\omega^2\rho[r,\theta]\sqrt{\frac{r^2+u^{(0,1)}[r,\theta]^2}{r^2}}\,u^{(0,2)}[r,\theta]}{r^3+r\,u^{(0,1)}[r,\theta]^2} +$$

$$\frac{ri^2\omega^2\nu[r,\theta]\rho[r,\theta]\sqrt{\frac{r^2+u^{(0,1)}[r,\theta]^2}{r^2}}\,u^{(0,2)}[r,\theta]}{r^3+r\,u^{(0,1)}[r,\theta]^2} + \frac{ro^2\omega^2\nu[r,\theta]\rho[r,\theta]\sqrt{\frac{r^2+u^{(0,1)}[r,\theta]^2}{r^2}}\,u^{(0,2)}[r,\theta]}{r^3+r\,u^{(0,1)}[r,\theta]^2} +$$

$$\frac{8\,ed^{(0,2)}[r,\theta]\,u^{(0,2)}[r,\theta]}{hr^3} + \frac{16\,u^{(0,1)}[r,\theta]\,\nu^{(0,1)}[r,\theta]\,ed^{(1,0)}[r,\theta]}{hr^2} - \frac{24\,u^{(0,2)}[r,\theta]\,ed^{(1,0)}[r,\theta]}{hr^2} -$$

$$\frac{r^4\omega^2\rho[r,\theta]\sqrt{1+\frac{u^{(0,1)}[r,\theta]^2}{r^2}}\,u^{(1,0)}[r,\theta]}{r^2+u^{(0,1)}[r,\theta]^2} + \frac{3\,ri^2\omega^2\rho[r,\theta]\sqrt{1+\frac{u^{(0,1)}[r,\theta]^2}{r^2}}\,u^{(1,0)}[r,\theta]}{r^2+u^{(0,1)}[r,\theta]^2} +$$

$$\frac{3\,r^2\,ri^2\omega^2\rho[r,\theta]\sqrt{1+\frac{u^{(0,1)}[r,\theta]^2}{r^2}}\,u^{(1,0)}[r,\theta]}{r^2+u^{(0,1)}[r,\theta]^2} + \frac{3\,ro^2\omega^2\rho[r,\theta]\sqrt{1+\frac{u^{(0,1)}[r,\theta]^2}{r^2}}\,u^{(1,0)}[r,\theta]}{r^2+u^{(0,1)}[r,\theta]^2} +$$

$$
\frac{3r^2 ro^2 \omega^2 \rho[r,\theta]\sqrt{1+\frac{u^{(0,1)}[r,\theta]^2}{r^2}}\,u^{(1,0)}[r,\theta]}{r^2+u^{(0,1)}[r,\theta]^2}-\frac{3r^4\omega^2\nu[r,\theta]\rho[r,\theta]\sqrt{1+\frac{u^{(0,1)}[r,\theta]^2}{r^2}}\,u^{(1,0)}[r,\theta]}{r^2+u^{(0,1)}[r,\theta]^2}+
$$

$$
\frac{ri^2\omega^2\nu[r,\theta]\rho[r,\theta]\sqrt{1+\frac{u^{(0,1)}[r,\theta]^2}{r^2}}\,u^{(1,0)}[r,\theta]}{r^2+u^{(0,1)}[r,\theta]^2}+\frac{r^2 ri^2\omega^2\nu[r,\theta]\rho[r,\theta]\sqrt{1+\frac{u^{(0,1)}[r,\theta]^2}{r^2}}\,u^{(1,0)}[r,\theta]}{r^2+u^{(0,1)}[r,\theta]^2}+
$$

$$
\frac{ro^2\omega^2\nu[r,\theta]\rho[r,\theta]\sqrt{1+\frac{u^{(0,1)}[r,\theta]^2}{r^2}}\,u^{(1,0)}[r,\theta]}{r^2+u^{(0,1)}[r,\theta]^2}+\frac{r^2 ro^2\omega^2\nu[r,\theta]\rho[r,\theta]\sqrt{1+\frac{u^{(0,1)}[r,\theta]^2}{r^2}}\,u^{(1,0)}[r,\theta]}{r^2+u^{(0,1)}[r,\theta]^2}+
$$

$$
\frac{8\,ed^{(0,2)}[r,\theta]u^{(1,0)}[r,\theta]}{hr^2}-\frac{8\,ed^{(1,0)}[r,\theta]u^{(1,0)}[r,\theta]}{hr}+\frac{16\,u^{(0,2)}[r,\theta]ed^{(1,0)}[r,\theta]\nu^{(1,0)}[r,\theta]}{hr}+
$$

$$
\frac{16\,ed^{(1,0)}[r,\theta]u^{(1,0)}[r,\theta]\nu^{(1,0)}[r,\theta]}{h}-\frac{16\,u^{(0,1)}[r,\theta]ed^{(1,1)}[r,\theta]}{hr^2}+\frac{16\,\nu[r,\theta]u^{(0,1)}[r,\theta]ed^{(1,1)}[r,\theta]}{hr^2}-
$$

$$
\frac{16\,\nu^{(0,1)}[r,\theta]ed^{(1,0)}[r,\theta]u^{(1,1)}[r,\theta]}{hr}+\frac{16\,ed^{(1,1)}[r,\theta]u^{(1,1)}[r,\theta]}{hr}-\frac{16\,\nu[r,\theta]ed^{(1,1)}[r,\theta]u^{(1,1)}[r,\theta]}{hr}+
$$

$$
\frac{16\,ed^{(1,0)}[r,\theta]u^{(1,2)}[r,\theta]}{hr}+\frac{8\,\nu[r,\theta]u^{(0,2)}[r,\theta]ed^{(2,0)}[r,\theta]}{hr}+\frac{8\,\nu[r,\theta]u^{(1,0)}[r,\theta]ed^{(2,0)}[r,\theta]}{h}+
$$

$$
\frac{8\,\nu[r,\theta]ed^{(0,2)}[r,\theta]u^{(2,0)}[r,\theta]}{hr}+\frac{16\,ed^{(1,0)}[r,\theta]u^{(2,0)}[r,\theta]}{h}+\frac{8\,\nu[r,\theta]ed^{(1,0)}[r,\theta]u^{(2,0)}[r,\theta]}{h}-
$$

$$
\frac{3r^3\omega^2\rho[r,\theta]u^{(2,0)}[r,\theta]}{\sqrt{1+u^{(1,0)}[r,\theta]^2}}-\frac{3ri^2\omega^2\rho[r,\theta]u^{(2,0)}[r,\theta]}{r\sqrt{1+u^{(1,0)}[r,\theta]^2}}+\frac{3r\,ri^2\omega^2\rho[r,\theta]u^{(2,0)}[r,\theta]}{\sqrt{1+u^{(1,0)}[r,\theta]^2}}-
$$

$$
\frac{3ro^2\omega^2\rho[r,\theta]u^{(2,0)}[r,\theta]}{r\sqrt{1+u^{(1,0)}[r,\theta]^2}}+\frac{3r\,ro^2\omega^2\rho[r,\theta]u^{(2,0)}[r,\theta]}{\sqrt{1+u^{(1,0)}[r,\theta]^2}}-\frac{r^3\omega^2\nu[r,\theta]\rho[r,\theta]u^{(2,0)}[r,\theta]}{\sqrt{1+u^{(1,0)}[r,\theta]^2}}-
$$

$$
\frac{ri^2\omega^2\nu[r,\theta]\rho[r,\theta]u^{(2,0)}[r,\theta]}{r\sqrt{1+u^{(1,0)}[r,\theta]^2}}+\frac{r\,ri^2\omega^2\nu[r,\theta]\rho[r,\theta]u^{(2,0)}[r,\theta]}{\sqrt{1+u^{(1,0)}[r,\theta]^2}}-\frac{ro^2\omega^2\nu[r,\theta]\rho[r,\theta]u^{(2,0)}[r,\theta]}{r\sqrt{1+u^{(1,0)}[r,\theta]^2}}+
$$

$$
\frac{r\,ro^2\omega^2\nu[r,\theta]\rho[r,\theta]u^{(2,0)}[r,\theta]}{\sqrt{1+u^{(1,0)}[r,\theta]^2}}+\frac{8\,r\,ed^{(2,0)}[r,\theta]u^{(2,0)}[r,\theta]}{h}-
$$

$$
\frac{1}{hr^3}\Big(16\,ed^{(0,1)}[r,\theta]\big(-u^{(0,3)}[r,\theta]+u^{(0,1)}[r,\theta]\big(-1+\nu[r,\theta]-r\,\nu^{(1,0)}[r,\theta]\big)-
r\big(\nu[r,\theta]u^{(1,1)}[r,\theta]+r\big(-\nu^{(1,0)}[r,\theta]u^{(1,1)}[r,\theta]+\nu^{(0,1)}[r,\theta]u^{(2,0)}[r,\theta]+u^{(2,1)}[r,\theta]\big)\big)\big)\Big)+
$$

$$
\frac{16\,r\,ed^{(1,0)}[r,\theta]u^{(3,0)}[r,\theta]}{h}+
$$

$$
\frac{1}{hr^3}\Big(8\,ed[r,\theta]\big(u^{(0,4)}[r,\theta]+r\,u^{(1,0)}[r,\theta]+2r\,\nu^{(0,1)}[r,\theta]u^{(1,1)}[r,\theta]-2r^2u^{(1,1)}[r,\theta]\nu^{(1,1)}[r,\theta]-
2u^{(0,1)}[r,\theta]\big(\nu^{(0,1)}[r,\theta]-r\,\nu^{(1,1)}[r,\theta]\big)-2r\,u^{(1,2)}[r,\theta]-r^2u^{(2,0)}[r,\theta]+r^2\nu^{(0,2)}[r,\theta]u^{(2,0)}[r,\theta]+
r^3\nu^{(1,0)}[r,\theta]u^{(2,0)}[r,\theta]+r^3u^{(1,0)}[r,\theta]\nu^{(2,0)}[r,\theta]+u^{(0,2)}[r,\theta]\big(4+r^2\nu^{(2,0)}[r,\theta]\big)+2r^2u^{(2,2)}[r,\theta]+
2r^3u^{(3,0)}[r,\theta]+r^4u^{(4,0)}[r,\theta]\big)\Big)
$$

The notations used here are as follows:

ri $\equiv r_i$, ro $\equiv r_o$, $\nu[r,\theta] \equiv \nu$, $\rho[r,\theta] \equiv \rho$, ed[r,θ] $\equiv D = \dfrac{Eh^3}{12\left(1-\nu^2\right)}$, u[r,θ] $\equiv u$,

and $\xi^{(p,q)}[r,\theta] \equiv \dfrac{\partial^{(p+q)}\xi}{\partial r^p\,\partial\theta^q}$ where ξ is D, ρ, ν or u for any p and q.

The above result was cross-checked by putting constant values of D, ρ and ν. It gave back the results as in [1] for disk with constant material properties.

The non-trivial solutions to this partial differential equation in r and θ with appropriate boundary conditions give the modal shapes of the rotating disk with inhomogeneous material properties like stiffeners, etc. And the corresponding ω_n's gives the natural frequencies.

3.5 Possibilities of solution

As it can be seen, the obtained differential equation is a pretty huge one and is difficult to handle analytically without any suitable approximations. Attempts were made to reduce the partial differential equation to ordinary ones using separation of variable method. The substitution $u(r,\theta) = u_1(r).u_2(\theta)$ was done, but without much simplification or separation of the variable r and θ. However there are possibilities of further investigation into the equation and solving it analytically using suitable methods.
However, as the present problem deals mainly with radial stiffeners (figure 4), a possible simplification of the equation may be performed by assuming that the properties like D, ρ and ν are functions of θ only.

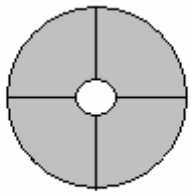

fig - 4

Moreover if we assume the stiffeners to be very thin and having drastically different material property values compared to that of the disk itself, the property functions D, ρ and ν may be approximated by a Dirac Delta function as follows:

$$\xi(r,\theta) = \xi_{disk} + \xi_{stiffner} \cdot \delta\left(\prod_{k=-n}^{n} \left(\theta - \frac{2\pi k}{n} \right) \right),$$

where, ξ is any property of the material integrated over length,
n = number of equispaced stiffeners on the disk.
It may be noted that the domain of θ in which all the analysis are done is assumed to be $[-2\pi, 2\pi]$.

4 Finite Element Analysis

The above partial differential equation can be attempted to be solved using suitable numerical techniques. However as a part of the present work, the numerical solutions have been performed using the FEM software Ansys. The description of the geometry, material properties, boundary conditions, grid type used, meshing and mode extraction method used are given below. All the values mentioned here are in SI unit system.

4.1 Geometry of the Disk

The disk was basically a thin annular cylinder with
internal radius(r_i) = 0.01, external radius(r_o) = 0.051, thickness(h) = 0.001.
The geometry and number of the stiffeners were varied and different sets of results were obtained for each of them.

4.2 Material Properties

The material of the disk is considered to be a type of plastic polymer, and the stiffeners were assumed to be made of steel. Hence the material property values were chosen accordingly.
The material of the disk was chosen to have the following properties:
$E = 40\times10^9$, $\rho = 2000$, $\nu = 0.25$
And the material of the stiffener was chosen to have the following properties:
$E = 200\times10^9$, $\rho = 7800$, $\nu = 0.3$

4.3 Boundary Conditions

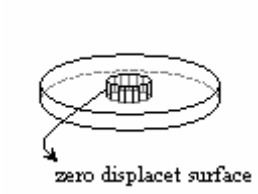

fig - 5

The boundary condition was set so as to ensure that the disk is clamped at it's inner circumference. In order to ensure that, the surface area of the inner cylinder of the disk was declared to have zero displacement along all the three degrees of freedom.

4.4 Grid type, meshing and mode extraction technique

For meshing the volume of the disk, the 20-nodes solid element 'SOLID95' provided in Ansys was chosen. The particular choice was made because the SOLID95 element can tolerate irregular shapes without much loss of accuracy and the elements have compatible displacement shapes and are well suited to model curved boundaries. Hence for the present problem dealing with thin circular disk, this element was found to be most suitable.
The meshing of both the disk and the stiffener volumes were done using unstructured grids. For the purpose of controlling the size of the elements Ansys's 'Smart Size' tool was used. For the volumes of the disk, the size level was set to 7 and for the stiffeners the size level was set to 6.
For each case, first a static analysis was performed with the prestressed effect on and with an angular velocity of the global coordinated about z-axis to account for the rotation of the disk. It was followed by a modal analysis with the previously obtained prestress data. For the modal analysis, the method used for extraction of the eigenvalues is Block Lanczos.

The following section describes the geometry, position and number of stiffeners used and the corresponding results obtained in each case.

5 Results

The standard mode shapes for disk without stiffeners and clamped at the inner circumference consists of nodal circumferences and nodal diameters. A mode shape with *i* nodal diameters and *j* nodal circles is termed as mode *(i, j)*. The following figures show some typical mode shapes (the lines represent the nodes):

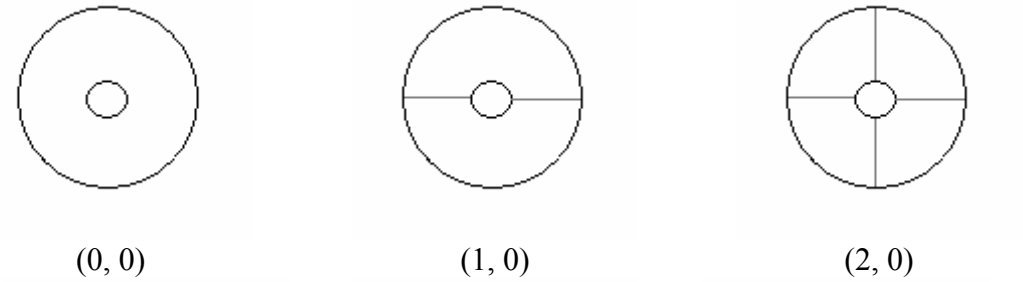

(0, 0) (1, 0) (2, 0)

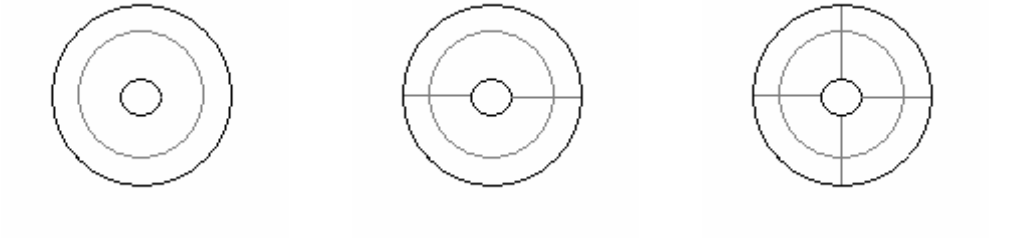

(0, 1) (1, 1) (2, 1)

fig – 6

5.1 Disk with no stiffeners

Modes obtained: First 20 modes were extracted, and the modal shapes obtained were the standard ones. A plot of the modal frequencies against the angular velocity of the disk is performed. The intersections of the straight lines with slopes 2, 3, etc with curves corresponding to modes (1,0), (2,0), etc give the critical frequencies. The following graph shows the plot for only the first 5 modes:

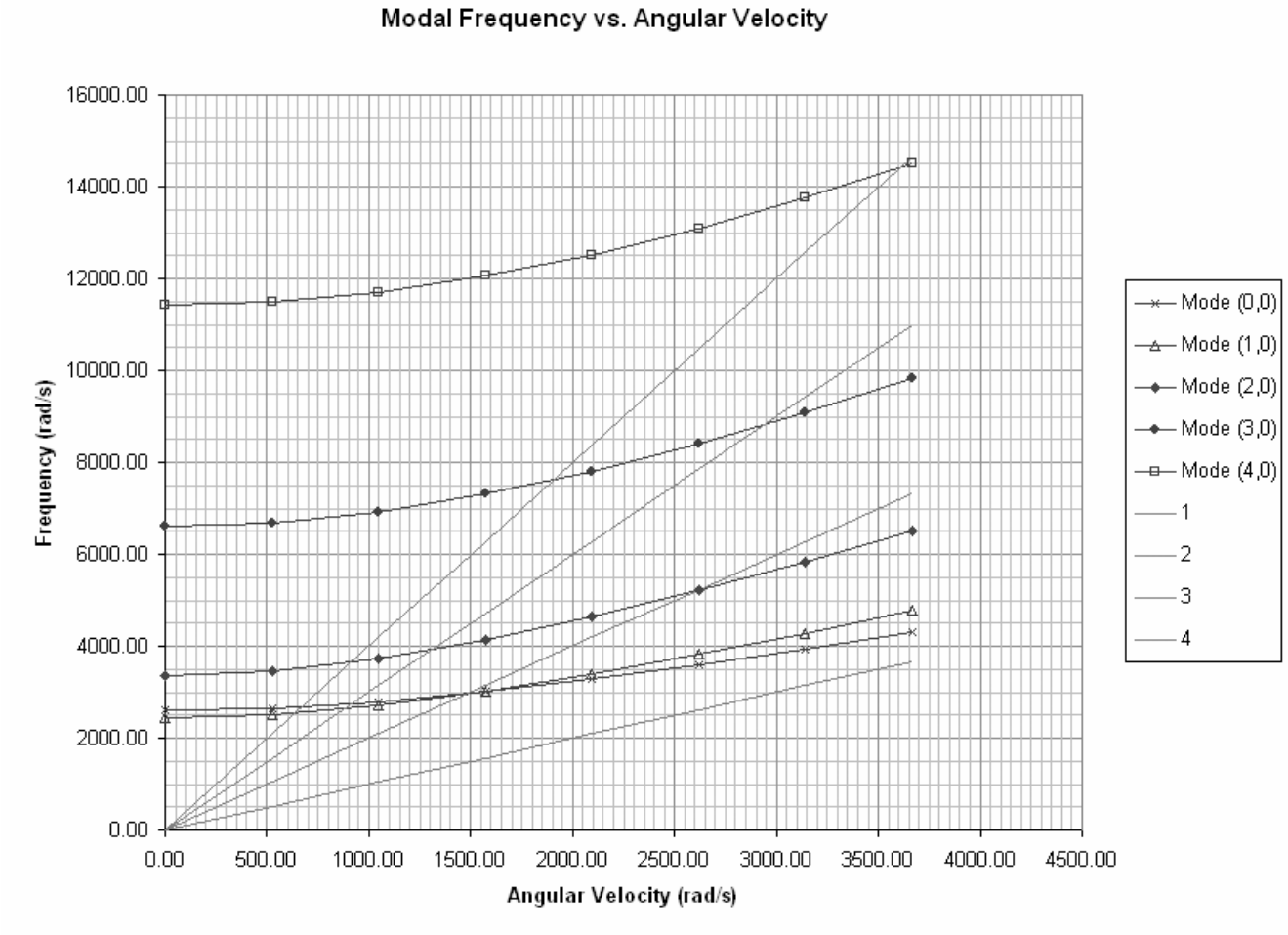

It was observed that the slope 1 line almost became asymptotic to the mode (0,0) curve. This is a result expected from the standard calculations for disk with no stiffeners.

5.2 Disk with three straight equispaced radial stiffeners

Stiffener Geometry: The stiffeners are simple thin rectangular parallelopipeds with length r_o-r_i = 0.041 and both height and thickness = h = 0.001.

Modes obtained: The mode shapes obtained were same as before, but for all the modes (i, j) with i as multiple of 3, the frequencies of the orthogonal modes got splitted. The splitted modes are denoted by 'A' for the modes which have stiffeners on antinodes and 'B' for the modes which have stiffeners on modal diameters.

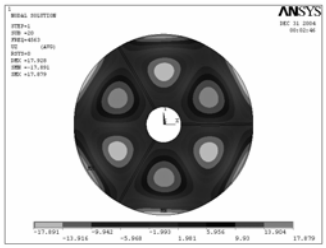

fig – 7 : A typical (3, 0) mode

Again, the plot of modal frequencies against the angular velocity was made.

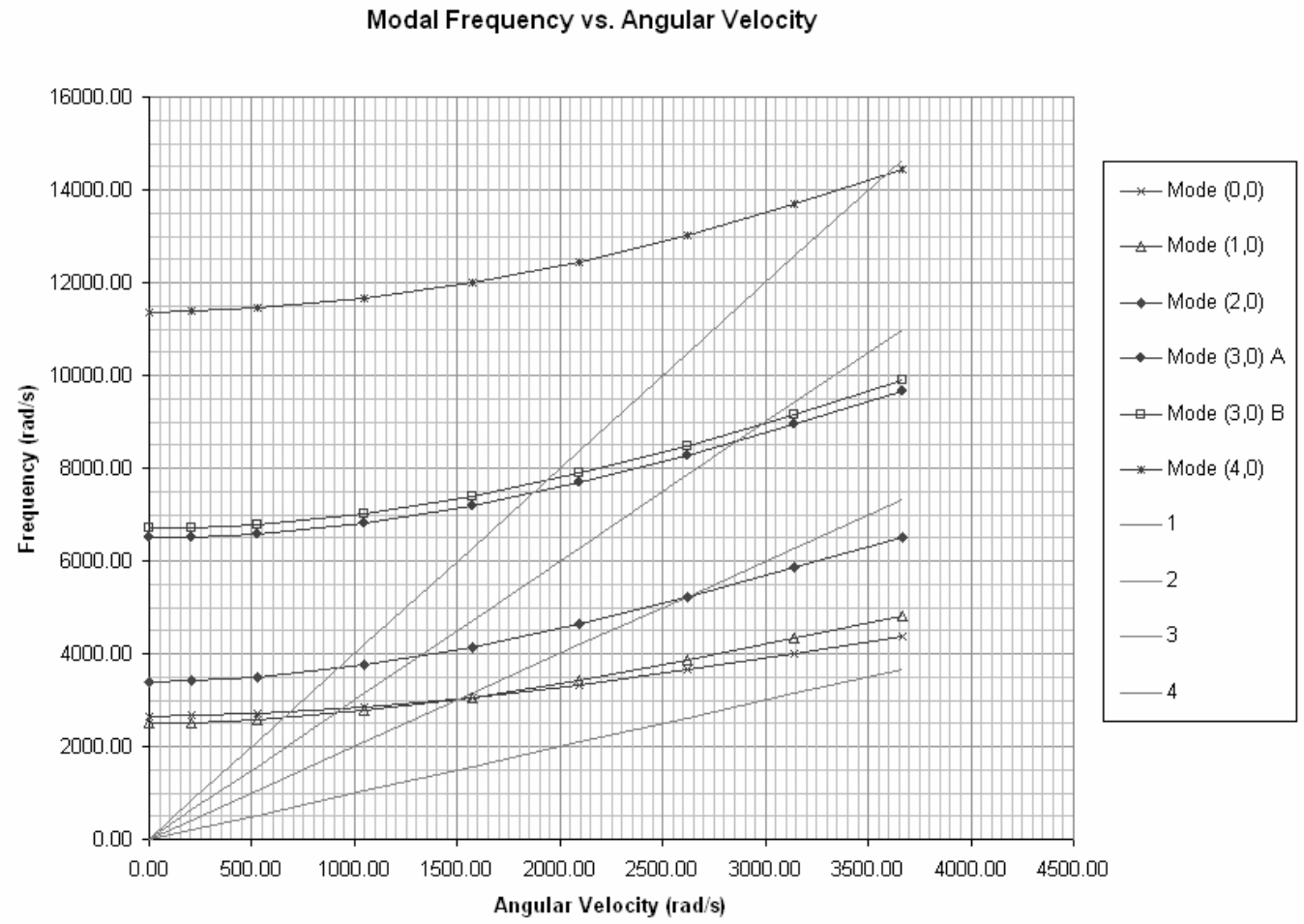

5.3 Disk with four straight equispaced radial stiffeners

Stiffener Geometry: Same as section 5.2.

Modes obtained: Mode shapes obtained were same as before, but splitting of orthogonal modes was observed for modes with nodal diameters multiples of 4.

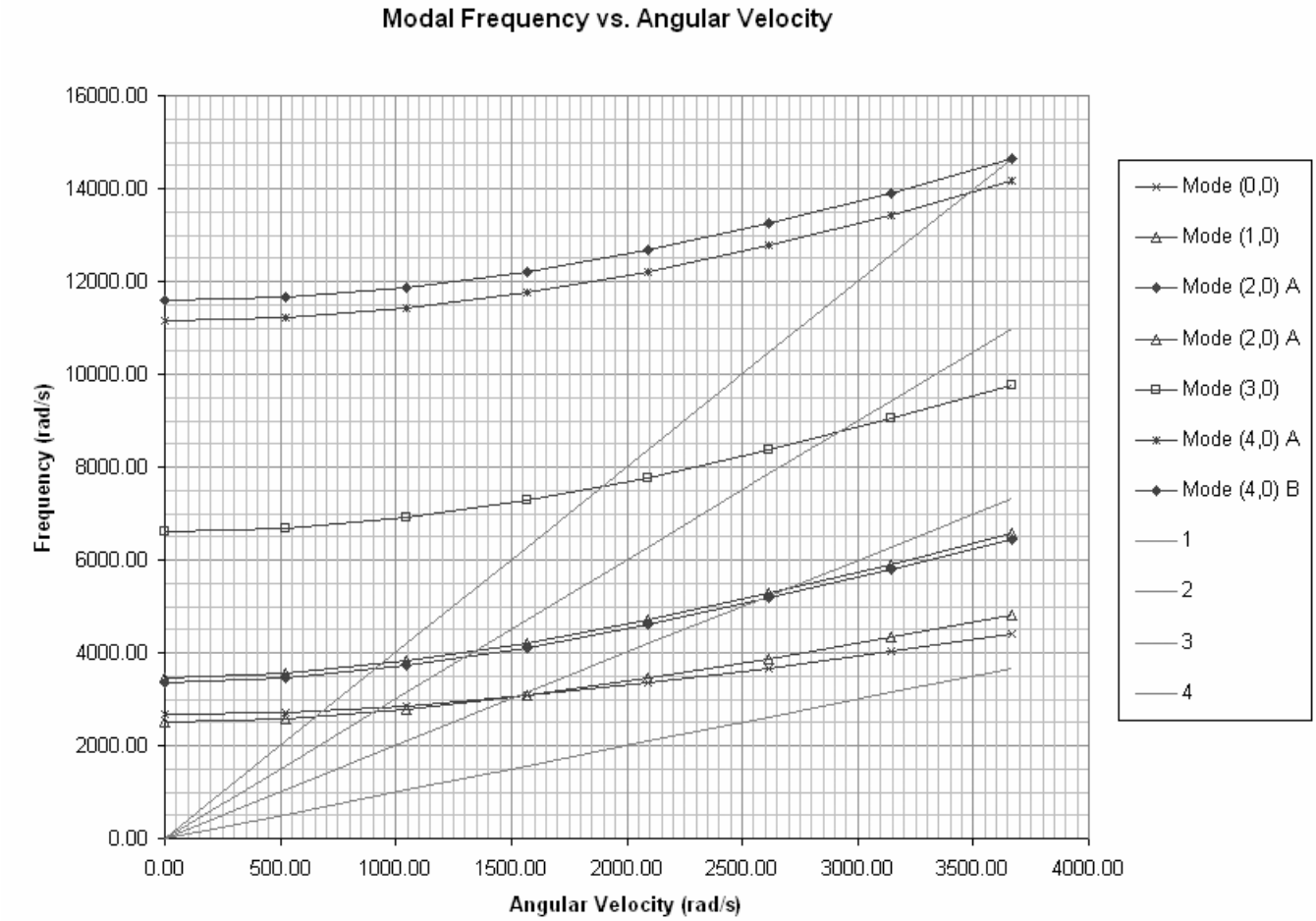

It may be observed here that till now there has not been any significant change in the critical angular velocities because of addition of stiffeners to the disk. Hence an investigation by altering the geometry of the stiffeners may be done to see if the critical angular velocities go up.
The following sections show the results obtained by altering the stiffener geometries.

5.4 Disk with three expanding (narrower near the inner circumference, wider near the outer circumference) equispaced radial stiffeners

Stiffener Geometry: The stiffeners are trapezoidal shaped thin blocks with width of 0.0004 at the inner circumference and 0.002 at the outer circumference.
The thickness is uniform thought and is equal to $h = 0.001$.

On starting the analysis with zero angular velocity of the disk, it was found that the modal frequencies, and hence the critical speeds decreased considerably compared to the straight stiffeners case. This as the undesired case, hence further continuation of analysis with this geometry of stiffener was discontinued.
However it was clear from the above mentioned observation that an increased mass concentration near the outer circumference is not desirable. Hence it may be interesting to do some study with stiffeners having higher mass concentration near the inner circumference.

5.5 Disk with three contracting (wider near the inner circumference, narrower near the outer circumference) equispaced radial stiffeners

Stiffener Geometry: As in 5.4, the stiffeners are the same trapezoidal shaped thin blocks, but they are now placed in a reverse orientation. That is, they have a width of 0.0004 at the outer circumference and 0.002 at the inner circumference.
The thickness is uniform thought and is equal to $h = 0.001$.

Modes obtained: Mode shapes obtained were similar to 5.2, with splitted orthogonal modes for modes with nodal diameters multiples of 3. However in this case, a few modes were found to be slightly deformed from the standard mode shapes.

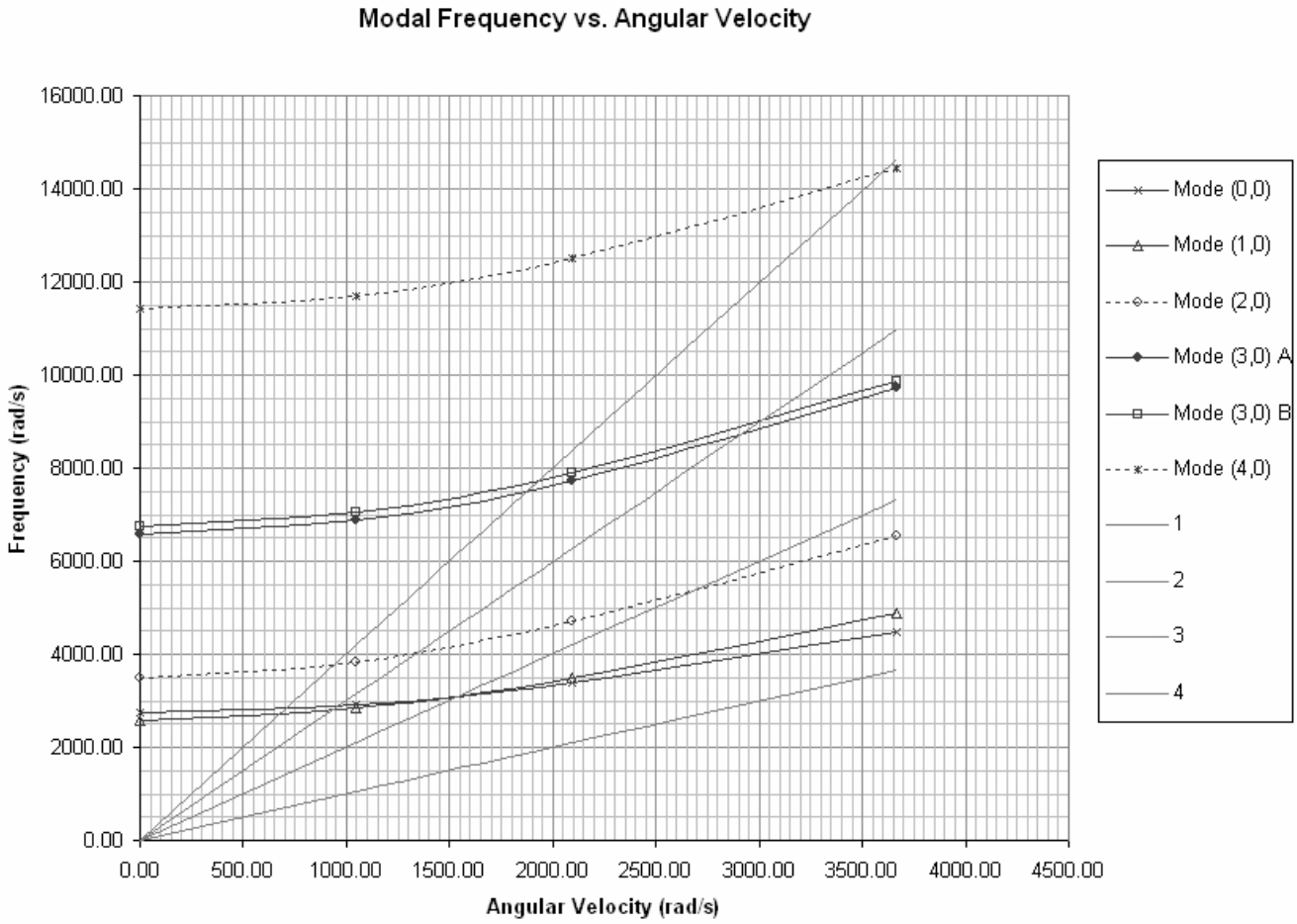

5.6 Intermediate Conclusions for proceeding with further modifications on the stiffener geometry

Though not very evident from the previous graphs, there had been a minor increase in the critical frequencies with contracting stiffeners when compared with the previous ones. A close comparative study of the frequencies of mode (1, 0) and its intersection with slope 2 line may reveal the fact.

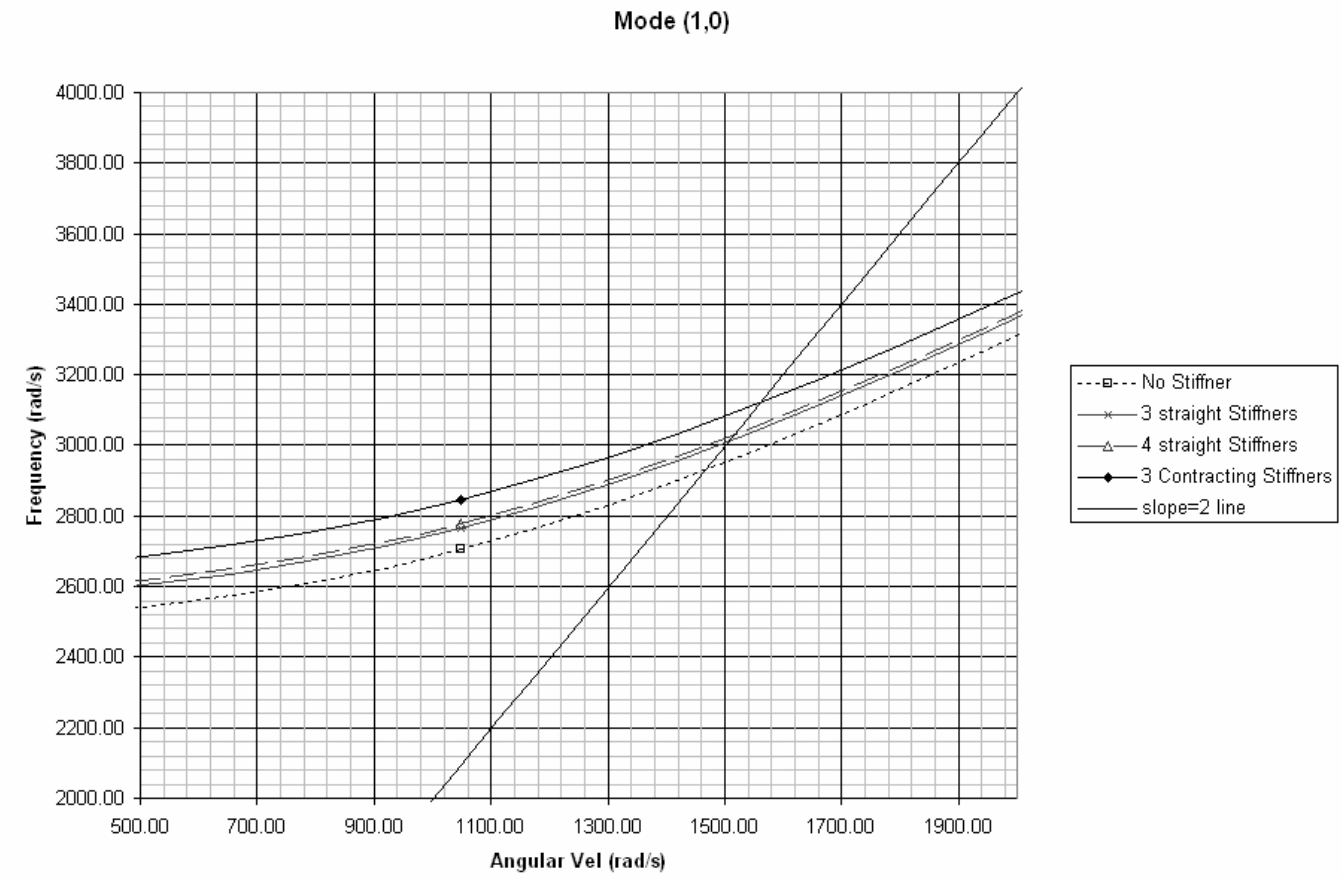

The above graph reveals:

- With addition of stiffeners, the lowest critical velocity has gone up slightly.
- By increasing the number of stiffeners from 3 to 4 not much difference id made on the critical velocities.
- By increasing the mass concentration of the stiffeners near the inner circumference there has been some increase in the critical velocity.
- However, in all the above mentioned cases the value of the first critical angular velocity lies within the value 1500 (± 50) rad/s. Hence nothing much has yet been achieved. Hence further investigation is required

From the above drawn conclusions it was logical to investigate the problem with stiffeners having even higher mass concentration near the inner circumference. The following section deals with such a stiffener geometry, which is a modification on the contracting stiffener, and was found to give much better results.

5.7 Disk with three raised, contracting (raised above the surface of the disk and wider near the inner circumference) equispaced radial stiffeners

Stiffener Geometry: The stiffeners are the similar to those of section 5.5, but they are now also raised above the surface of the disk near the inner circumference and gradually slopes down to meet the disk surface at the outer circumference. Hence, they are a sort of truncated pyramidal shaped stiffeners with the base of the pyramid at the inner circumference, and apex at the outer circumference.
At the inner circumference they have a width of 0.002 and thickness of 0.00512.
And at the outer circumference they have a width of 0.0004 and thickness of 0.001.
Thus the geometry appears something as shown below (figure not to the scale):

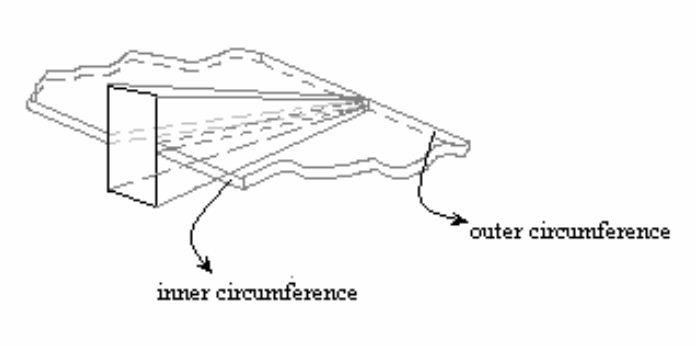

fig – 8

Modes obtained: In this case the mode shapes obtained were rather very interesting. Apart from a few standard higher mode shapes (like (4,0), (5,0), (6,0) and (3,1)), a few new types of modes were obtained, some of which were much deformed an asymmetric.
It was interesting to observe that the standard modes with the lower modal frequencies were completely replaced by new modes with much higher modal frequencies. Hence the first few critical speeds of the disk were expected to increase considerably.

The results obtained follows.

As only a few of the standard modes were available, they are shown in the following graph:

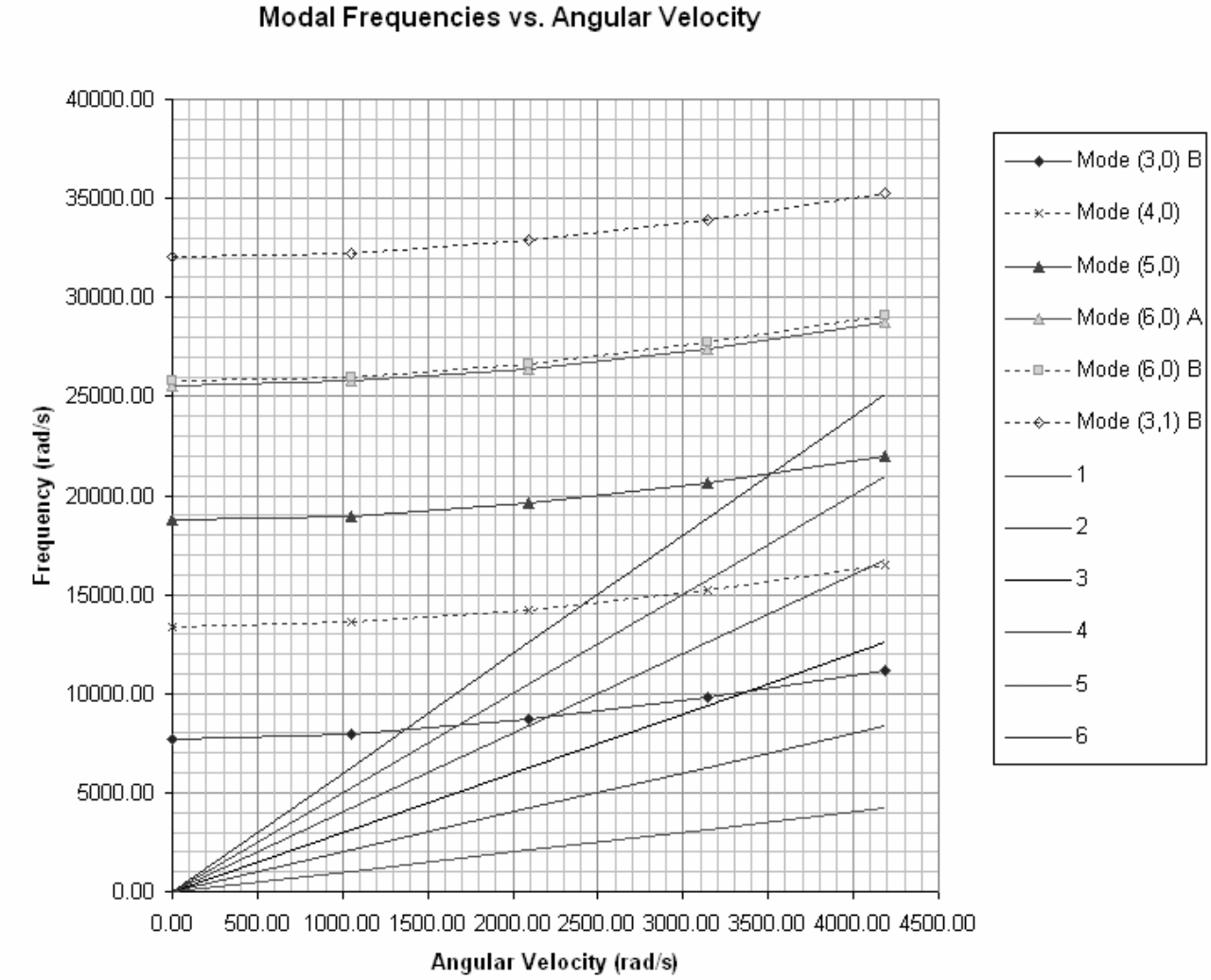

But it will be of greater interest to make a study on the new mode shapes obtained with the present stiffener geometry. The following figures show some of those mode shapes:

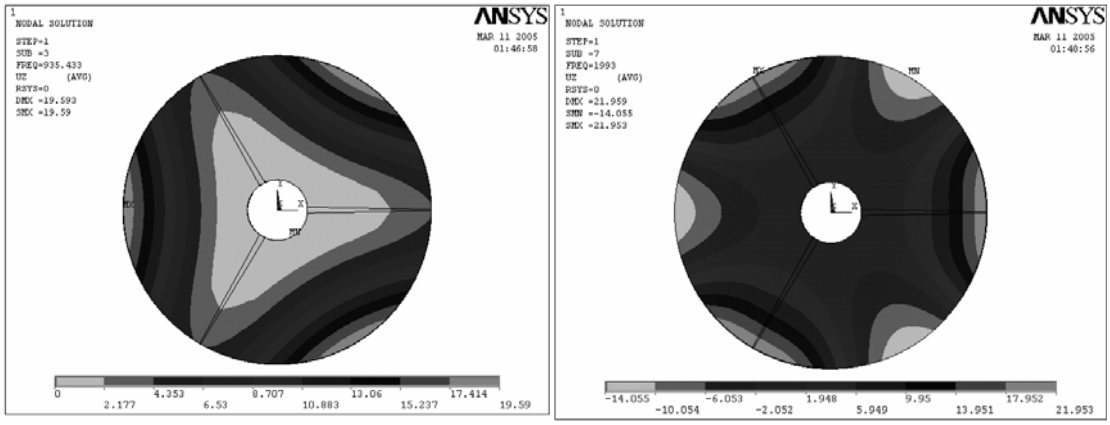

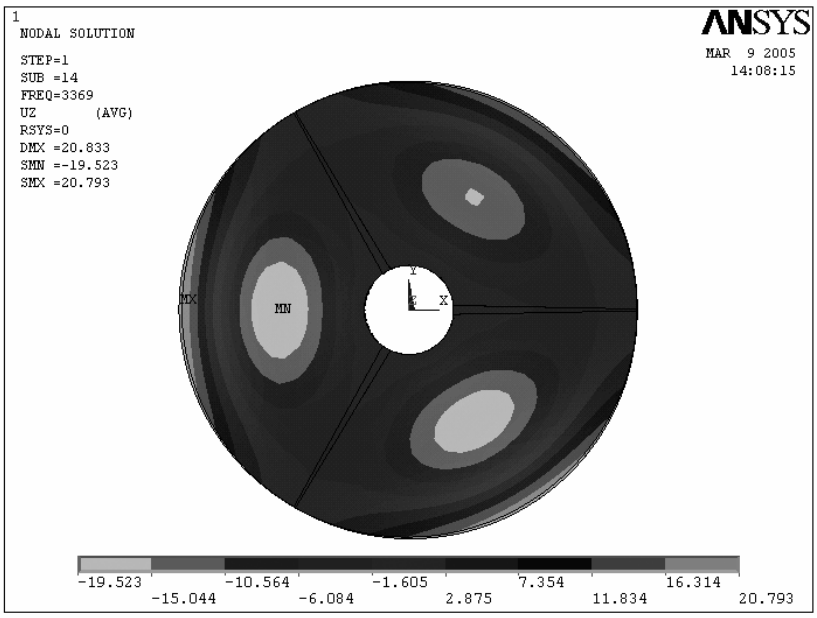

fig – 9 : Unusual mode shapes obtained

As most of the standard (*i, j*) modes are absent with the present stiffener geometry, we will term the modes mode-1, mode-2, etc. in ascending order of their modal frequencies. For the purpose of comparison with the other stiffener geometries the modal frequency vs. angular velocity graphs were plotted for the different stiffeners for mode-1, mode-2 and mode-3.

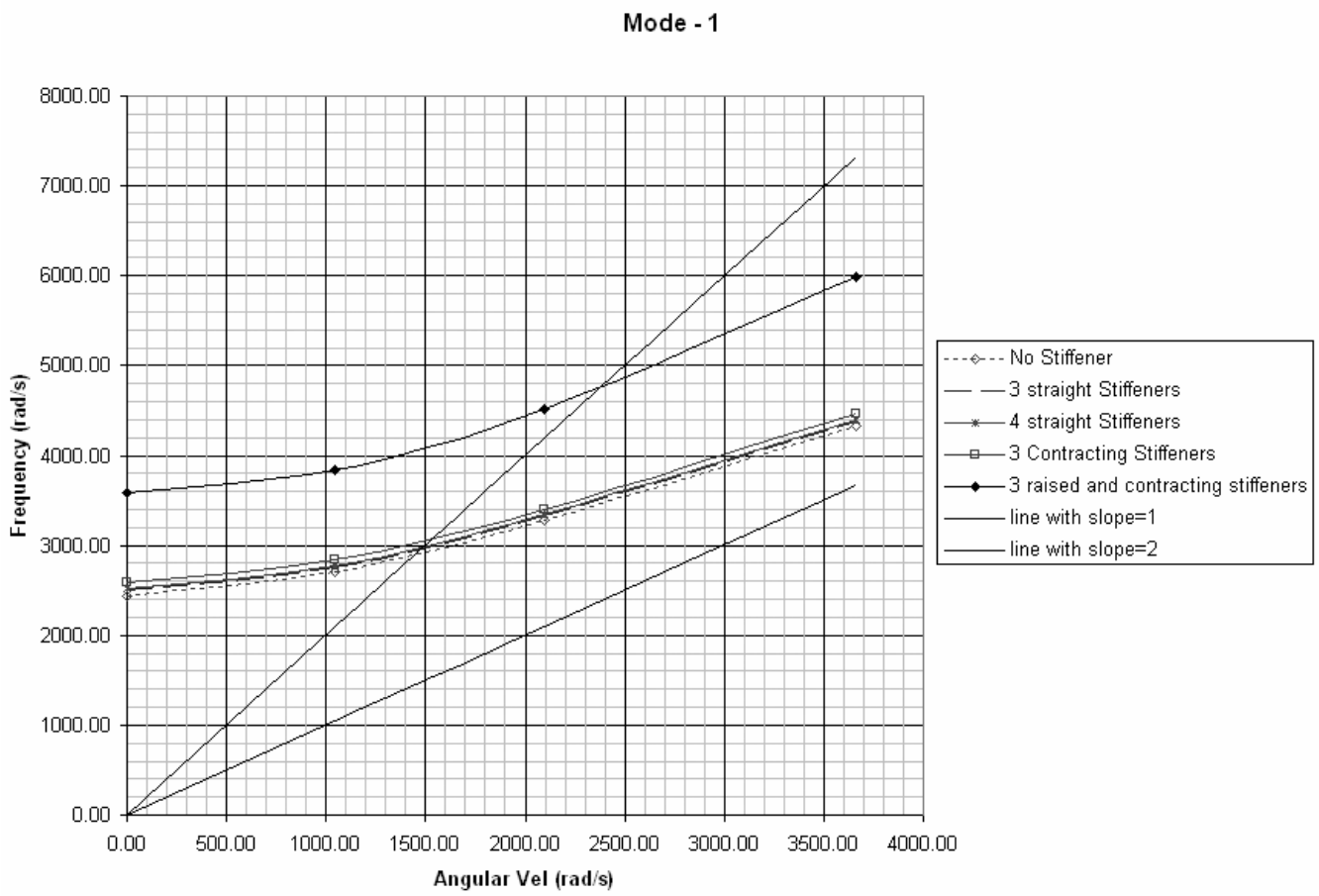

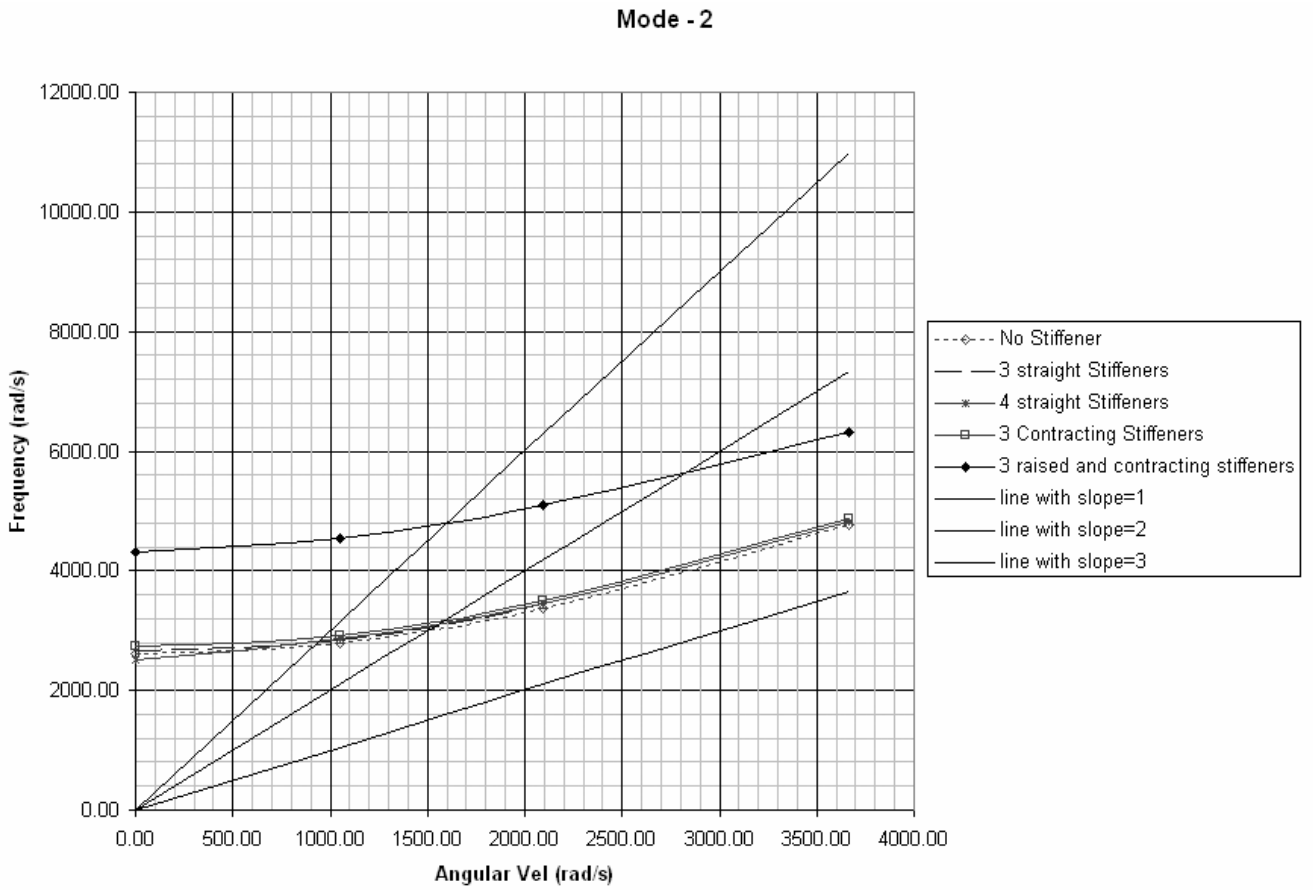
Mode - 2
12000.00
10000.00
8000.00
6000.00
4000.00
2000.00
0.00
Frequency (rad/s)
0.00
500.00
1000.00
1500.00
2000.00
2500.00
3000.00
3500.00
4000.00
Angular Vel (rad/s)
No Stiffener
3 straight Stiffeners
4 straight Stiffeners
3 Contracting Stiffeners
3 raised and contracting stiffeners
line with slope=1
line with slope=2
line with slope=3

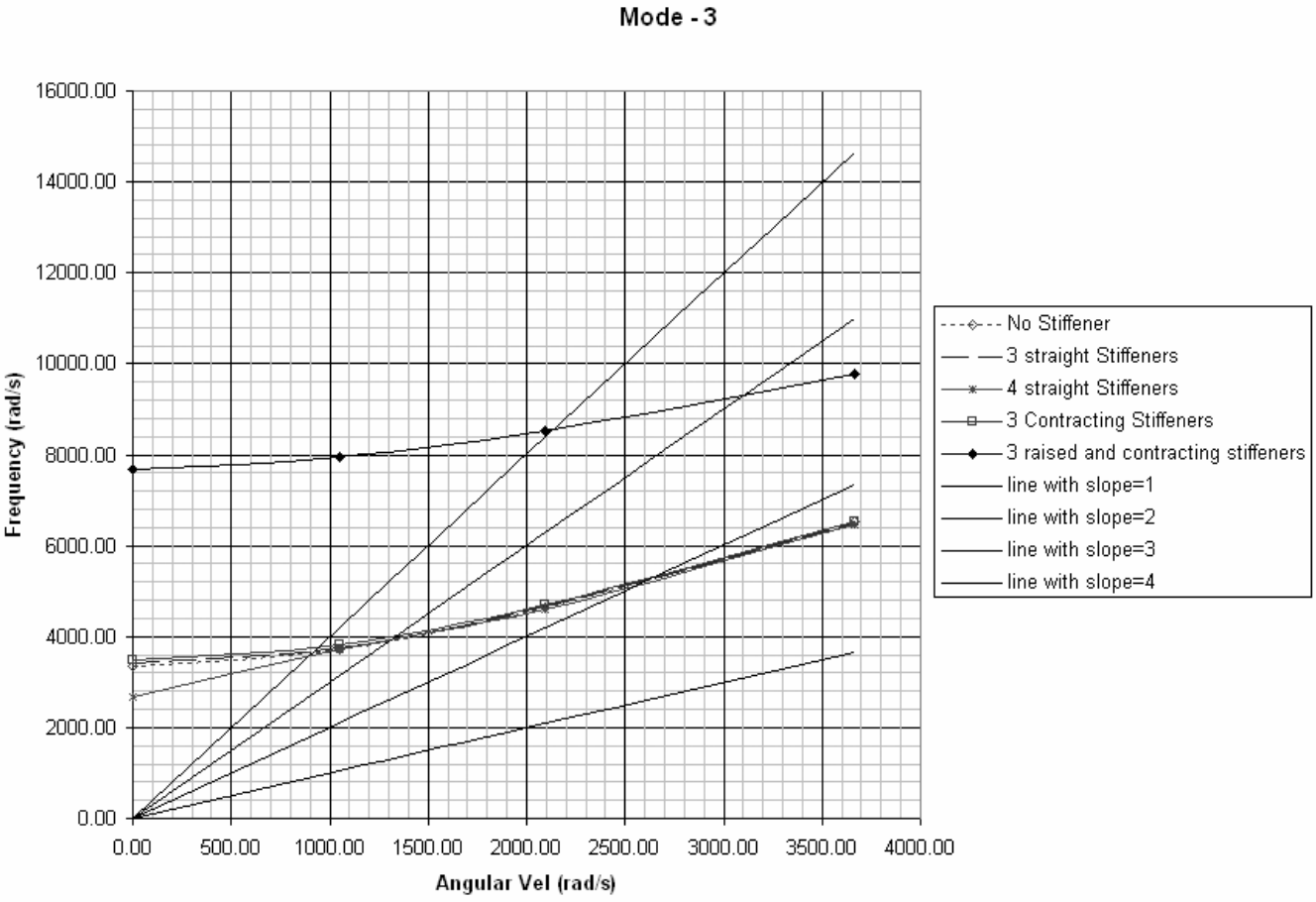
Mode - 3
16000.00
14000.00
12000.00
10000.00
8000.00
6000.00
4000.00
2000.00
0.00
Frequency (rad/s)
0.00
500.00
1000.00
1500.00
2000.00
2500.00
3000.00
3500.00
4000.00
Angular Vel (rad/s)
No Stiffener
3 straight Stiffeners
4 straight Stiffeners
3 Contracting Stiffeners
3 raised and contracting stiffeners
line with slope=1
line with slope=2
line with slope=3
line with slope=4

From the above graphs it can easily be seen how the 3 contracting and raised stiffeners used in this section have increased the modal frequencies for the disk substantially.
However, as many of the standard modes were absent, it is difficult to draw any immediate conclusions regarding the critical speed of the disk. But as the modal frequencies were found to increase considerably, one can logically expect the critical velocities to increase accordingly.
Hence the raised contracting stiffener gave extremely desirable results by increasing the modal frequencies. Even if we keep some allowance in these results in order to account for the numerical errors caused due to difference in meshing, the results show a high potential for the success of the stiffener geometry mentioned in 5.5.

However some of the mode shapes obtained in the simulation of 5.5 were highly deformed and asymmetric. This may be because of numerical errors caused by uneven meshing, limitations of the mode extraction and solving methods used, etc. Further investigation is possible in order to explain these anomalous modal shapes.

6 Conclusions

The final conclusions that can be drawn from the above analysis and results:

- An analytical solution has been attempted in order to account for variation of material properties within the disk, which is in fact the case for disks with stiffeners. A differential equation has been successfully set up and cross-checked by putting constant values of material properties to obtain the equation in [1]. However a final solution could not be achieved at the present moment due to the complexity of the differential equation. Further studies on the obtained partial differential equation with appropriate approximations may lead to a satisfactory analytical solution.

- Using the FEM software Ansys, modal analysis of the rotating disk with stiffeners of different geometries were performed. A gradual development of the stiffener geometries on the basis of conclusions drawn from intermediate results finally yielded a stiffener which could successfully push up the modal frequencies, and hence potentially increase the critical speeds of the disk.

- Further investigation into the problem may result in a successful analytical method for dealing with such disks with stiffeners. Moreover variation in the dimensions and geometry of the obtained stiffener may yield better and interesting results.

7 References

[1] S.Timoshenko and S.W.Krieger, *Theory of Plates and Shells*, Prentice Hall.

[2] Egor Popov, (1973), *Introduction to Mechanics of Solids*, Delhi, Printice Hall.

[3] Erwin Kreyszig, *Advanced Engineering Mathematics*, John Wiley & Sons Inc.